Ecotoxicology and Environmental Safety 236 (2022) 113500

Contents lists available at ScienceDirect

Ecotoxicology and Environmental Safety

journal homepage: www.elsevier.com/locate/ecoenv

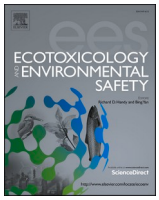

Impaired V-ATPase leads to increased lysosomal pH, results in disrupted lysosomal degradation and autophagic flux blockage, contributes to fluoride-induced developmental neurotoxicity

Xie Han [a,b,c,d,1], Yanling Tang [a,b,c,d,1], Yuanli Zhang [a,b,c,d], Jingjing Zhang [a,b,c,d], Zeyu Hu [a,b,c,d], Wanjing Xu [a,b,c,d], Shangzhi Xu [a,b,c,d], Qiang Niu [a,b,c,d,*]

[a] Department of Preventive Medicine, School of Medicine, Shihezi University, Shihezi, Xinjiang, People's Republic of China
[b] Key Laboratory of Preventive Medicine, Shihezi University, Shihezi, Xinjiang, People's Republic of China
[c] Key Laboratory of Xinjiang Endemic and Ethnic Diseases (Ministry of Education), School of Medicine, Shihezi University, Shihezi, Xinjiang, People's Republic of China
[d] NHC Key Laboratory of Prevention and Treatment of Central Asia High Incidence Diseases (First Affiliated Hospital, School of Medicine, Shihezi University), People's Republic of China

ARTICLE INFO

Edited by Dr Yong Liang

Keywords:
Fluoride
V-ATPase
Lysosomal pH
Lysosomal degradation capacity
Developmental neurotoxicity

ABSTRACT

Fluoride is capable of inducing developmental neurotoxicity, yet its mechanisms remain elusive. We aimed to explore the possible role and mechanism of autophagic flux blockage caused by abnormal lysosomal pH in fluoride-induced developmental neurotoxicity, focusing on the role of V-ATPase in regulating the neuronal lysosomal pH. Using Sprague-Dawley rats exposed to sodium fluoride (NaF) from gestation through delivery until the neonatal offspring reached six months of age as an *in vivo* model. The results showed that NaF impaired the cognitive abilities of the offspring rats. In addition, NaF reduced V-ATPase expression, diminished lysosomal degradation capacity and blocked autophagic flux, and increased apoptosis in the hippocampus of offspring. Consistently, these results were validated in SH-SY5Y cells incubated with NaF. Moreover, NaF increased the SH-SY5Y lysosomal pH. Mechanistically, V-ATPase B2 overexpression and ATP effectively restored V-ATPase expression, reducing NaF-induced lysosomal alkalinization while increasing lysosomal degradation capacity. Notably, those above pharmacological and molecular interventions diminished NaF-induced apoptosis by restoring autophagic flux. Collectively, the present findings suggested that NaF impairs the lysosomal pH raised by V-ATPase. This leads to reduced lysosomal degradation capacity and triggers autophagic flux blockage and apoptosis, thus contributing to neuronal death. Therefore, V-ATPase might be a promising indicator of developmental fluoride neurotoxicity.

1. Introduction

Fluoride is widespread and unevenly distributed in the environment, and it can be rapidly absorbed into the body *via* water, food, and air (Johnston and Strobel, 2020). Fluoride consumption at the prescribed level is essential for human health, whereas excessive fluoride exposure is harmful to health. Groundwater, minerals, soil, household chemical products such as varnishes, gels, mouthwashes, and toothpaste are significant sources of fluoride exposure. Others include industrial emissions and pesticide residues. (Lacson et al., 2020; Wang et al., 2019). Indeed, fluoride exposure in drinking water is the leading cause of fluorosis, threatening both skeletal and non-skeletal organs such as the liver, kidney, testes, thyroid, and brain (Johnston and Strobel, 2020; Yadav et al., 2018). The neurological system is the primary target of fluoride damage in humans (Dec et al., 2017). Neurotoxicants cause more damage to the developing brain than adult brain (Dobbing, 1971).

Abbreviations: V-ATPase, vacuolar H^+-ATPase; Cath-D, cathepsin D; LC3, microtubule-associated protein 1 light chain 3; p62, sequestosome 1; PARP, poly ADP-ribose polymerase 1; DQ-BSA, self-quenched Bodipy-conjugated bovine serum albumin; DMEM, Dulbecco's modified eagle's medium; FBS, fetal bovine serum; ATP, adenosine triphosphate; Ad, adenovirus; BaF, bafilomycin A1.

* Correspondence to: Department of Preventive Medicine, School of Medicine, Shihezi University, North 2th Road, Shihezi, Xinjiang 832000, People's Republic of China.
E-mail address: niuqiang@shzu.edu.cn (Q. Niu).

[1] Xie Han[1] and Yanling Tang[1] equally contributed to this research.

https://doi.org/10.1016/j.ecoenv.2022.113500
Received 10 December 2021; Received in revised form 31 March 2022; Accepted 6 April 2022
Available online 11 April 2022
0147-6513/© 2022 The Authors. Published by Elsevier Inc. This is an open access article under the CC BY-NC-ND license (http://creativecommons.org/licenses/by-nc-nd/4.0/).

Fluorine can penetrate both the placental barrier and the blood-brain barrier (BBB) and enter the fetal brain (Atlanta. Agency for Toxic Substances and Disease Registry ATSDR, 2003). Noteworthy, infants and children retain more absorbed fluoride than adults (O'Mullane et al., 2016; Avvannavar, 2007). Prolonged exposure leads to fluoride accumulation in the brain, and consequent nervous system damage (Su et al., 2021). Epidemiological cross-sectional and prospective studies have found that fluoride exposure can negatively impact children (Valdez et al., 2017; Yu et al., 2018). In *in vivo* trials, embryonic and lactational exposure to fluoride alters the neurological functions of rats, resulting in decreased learning and memory capacity (Xin et al., 2021; Cao et al., 2019). *In vitro* studies have also documented biochemical changes induced by fluoride in brain cells, such as lipid peroxidation and inflammatory responses (Gao et al., 2008; Goschorska et al., 2018). Despite emerging evidence that fluoride exposure causes neurological development damage, the detailed mechanism underlying fluoride-induced developmental neurotoxicity is still largely unclear.

Due to their nonrenewable nature, neurons are unable to mitigate the load of harmful substances accumulated in the cells. Therefore, autophagy plays a dominant role in sustaining neuronal homeostasis by rapidly removing such substances (Shaikh et al., 2021). Autophagy is classified based on the pathways of degradation substrates into autolysosomes as macroautophagy, microautophagy, and chaperone-mediated autophagy (Mizushima and Levine, 2020). Macroautophagy, commonly referred to as autophagy, is a key intracellular degradation process. (Jimenez-Moreno and Lane, 2020). The dynamic process of autophagy is known as autophagic flux and involves several basic steps: autophagosome biogenesis and maturation, fusion of autophagosomes with lysosomes, and degradation of autophagic substrates within lysosome (Nie et al., 2021). Autophagic flux blockage results in the accumulation of pathogenic and misfolded proteins, as well as damaged organelles, resulting in neuronal damage that underlies various neurological disorders (Blumenreich et al., 2020). Fluoride triggers defective autophagy and causes excessive apoptosis in human neuroblastoma SH-SY5Y cells, thus resulting in neurotoxicity (Zhou et al., 2019). We previously found that sodium fluoride (NaF) causes autophagic flux blockage, apoptosis, and reduced viability in SH-SY5Y cells and the Sprague-Dawley (SD) rat hippocampus (Niu et al., 2018). Chloroquine (inhibitor of autophagic degradation) exacerbated, whereas rapamycin (autophagy agonist) attenuated the reduced viability of SH-SY5Y cells caused by NaF (Niu et al., 2018). Although autophagic flux blockage is associated with fluoride-induced developmental neurotoxicity, the underlying mechanisms remain unknown.

Lysosomes are important subcellular organelles that receive and degrade macromolecules through endocytosis and autophagy (Zhang et al., 2021). The degraded products are transported out of lysosomes *via* membrane trafficking for reuse or energy production (Rudnik and Damme, 2021). Lysosomal degradation capacity is mainly dependent on more than 60 active hydrolases in their lumen, which catalyze the hydrolysis process to breakdown biomolecules (Trivedi et al., 2020). An acidic environment (pH 4.5–5.0) within the lysosomal lumen is vital for lysosomal degradation capacity by keeping the optimal environment for soluble hydrolases (Yamamoto et al., 2021). Ion channels and proton pumps are paramount in sustaining an acidic environment during lysosomal acidification. Vacuolar adenosine triphosphatase (V-ATPase) is a pH-sensitive multisubunit proton transporter that establishes and maintains an acidic environment within the lysosome by using the energy of ATP hydrolysis to pump H^+ into the lysosome (Liu et al., 2021). Changes in V-ATPase expression and activity and abnormal lysosomal pH are associated with various neurodegenerative diseases, such as Alzheimer's and Parkinson's diseases (Colacurcio and Nixon, 2016). However, the involvement of abnormal lysosomal pH in neurological damage induced by fluoride and the role and mechanism of V-ATPase in regulating lysosomal pH has not been clarified.

Therefore, we aimed to determine the role and mechanism of the lysosomal pH abnormalities that cause autophagic flux blockage in developmental fluoride neurotoxicity, particularly focusing on the involvement of V-ATPase in regulating lysosomal pH in neurons. Rats were given fluoridated drinking water *ad libitum* from the time of gestation, through delivery until the neonatal offspring reached the age of six months (simulating human exposure during a critical period of neurological development), and an *in vitro* model of NaF-treated SH-SY5Y cells, a cell line widely used to study developmental neurotoxicity. We explored the targets and molecular mechanism of fluoride-induced developmental neurotoxicity from the perspective of abnormal lysosomal pH leading to autophagic flux blockage. We also aimed to provide theoretical and scientific foundations for the prevention and treatment of fluorosis.

2. Materials and methods

2.1. Chemical reagents

NaF was obtained from Sigma (USA). Bafilomycin A1 (BaF) was obtained from Selleckchem (USA). ATP was purchased from Shanghai Acmec Biochemical Co., Ltd. (China). Dulbecco's modified eagle's medium was obtained from Gibco (USA). Fetal bovine serum was purchased from Biological Industries (USA). BCA assay kit and RIPA lysis buffer were obtained from Beyotime Biotechnology Ltd. (China). V-ATPase B2 antibodies were provided by Santa Cruz Biotechnologies (USA). Cathepsin D, LC3, p62, PARP, and GAPDH antibodies were obtained from Proteintech (USA). β-actin antibody was provided by Boster Co., Ltd. (China). LysoSensor™ Yellow/Blue DND-160 (PDMPO) was purchased from Yeasen Ltd. (China), DQ™-Green-BSA was purchased from Thermo Fisher (USA), and Annexin V-FITC/PI apoptosis detection kit was purchased from MultiSciences Biotech Co. (China), Cathepsin D activity detection kit was purchased from Jianglai Biological Technology Co., Ltd. (China), mRFP-GFP-LC3 adenoviral vectors were provided by Hanbio Biotechnology Co., Ltd. (China), and recombinant adenovirus plasmid expressing V-ATPase B2 was provided by WZ Biosciences Inc. (China).

2.2. Experiment model and treatments

Adult SD rats (180–250 g) were purchased from the Experimental Animal Center of Xinjiang Medical University, license number: SCXK (Xinjiang) 2018–0003. Rats were housed in a room with constant temperature (20–25 ℃) and humidity (50%−60%) under a 12 h light/dark cycle. Experiments described in this study were approved by the Animal Research Ethics Committee of the School of Medicine, Shihezi University. After acclimation, rats were randomly divided into four groups: one control group (tap water, containing less than 1.0 mg/L fluorine) and three NaF-treated groups (NaF was received at 25, 50, or 100 mg/L in drinking water, and the corresponding fluorine content is 11.3, 22.6, or 45.2 mg/L, respectively). Furthermore, according to the conversion of animal doses to human equivalent doses based on body surface area, fluoride concentrations in drinking water for rats need to be five times higher than humans to achieve the same final concentration (Program, 2016). Therefore, the dosages of NaF chosen for this study are reasonable, and the environmental relevance of these dosages has also been discussed in our previous study (Niu et al., 2018; Zhao et al., 2020). The male and female rats were then caged and mated ($n = 15$ per group, the ratio of males to females was 2:1), and vaginal suppositories were checked every morning to determine pregnancy. Pregnant female rats were placed in individual cages and continuously exposed to NaF by drinking water throughout the gestation and subsequent lactation. The offspring were weaned on postnatal day (PND) 21, and continually exposed to NaF by drinking water at the same concentration as the parental rats. On PND 180, the offspring were randomly selected from each group (the ratio of females to males was 1:1) for the Morris water maze (MWM) test. Then, the rats were sacrificed after overnight fasting. Hippocampal samples were collected immediately at 4 ℃. From each

group, three samples were embedded in paraffin, and the others were kept at - 80 ℃ for further biochemical analysis.

2.3. MWM test

The MWM (XR-XM101, China) instrument consists of a circular pool (1.8 m diameter and 0.5 m height), a platform (black cylinder, 8 cm diameter and 30 cm height) underwater placed at a fixed position in the target quadrant, and a camera above the center of the pool to capture images of swimming rats and connected to the tracking system. The pool was filled with water (temperature was kept at 24 ± 1 ℃) until it exceeds the platform by 2 cm and mixed with non-toxic black ink to make the water black to hide the platform.

The MWM test consists of a positioning and navigation test (PNT) and a space detection test (SPT). In the PNT, rats faced the wall and gently placed into the pool and were allowed to swim freely. If the platform was found within 60 s, the time was recorded as the escape latency and the rat was allowed to stand on the platform for 10 s. If not, the rat was allowed to stand on the platform for 15 s, and the escape latency of rat was recorded as 60 s. Every rat was placed once in each quadrant per day for 4 consecutive days. The following results were recorded: escape latency, swimming speed, swimming distance and swimming route. In the SPT, the platform was removed, and the rat was forced to swim for 60 s in the pool freely. The following results were recorded: the frequency of platform crossing, the duration spent in the target quadrant, the swimming distance, and the swimming route.

2.4. Nissl staining

Paraffin-embedded samples were sliced into 4 μm-thick sections, separated in xylene, dehydrated in gradient ethanol (95%, 85%, and 70%) for 5 min, stained with 1% cresyl violet stain for 40 min, and washed 3 times with distilled water. Then, the sections were infiltrated in 95% alcohol for 5 min, washed with xylene and covered with neutral gel, and finally observed with a microscope (Japan).

2.5. Cell culture and treatment

Human neuroblastoma SH-SY5Y cells were obtained from American Type Culture Collection (USA), cultured in DMEM supplemented with 10% fetal bovine serum (FBS), 100 U/ml penicillin, and 100 g/ml streptomycin, and incubated in an incubator with a humidified atmosphere containing 5% CO_2 in air at 37 ℃. When cells grew to 80% confluence in the culture dish or plate, the cells were treated with NaF (20, 40, or 60 mg/L) for 24 h (the dosages in the present experiment were based on our previous study (Niu et al., 2018)). In addition, the BaF (100 nmo/L) or ATP (1 μmol/L) was pretreated with cells for 1 h, respectively, followed by treatment with NaF (60 mg/L) for another 24 h. Meanwhile, the cells were transduced with recombinant adenovirus plasmid expressing V-ATPase B2 (MOI = 200) or adenoviruses control (Ad-null). After being infected with Ad-V-ATPase B2 or Ad-null for 24 h, SH-SY5Y cells were treated with NaF (60 mg/L) for another 24 h.

2.6. Measurement of lysosomal pH

The LysoSensor™ Yellow/Blue DND-160 Kit (Yeasen) was used according to the manufacturer's protocol. Briefly, cells were seeded on coverslips in a 24-well plate and treated with NaF for 24 h, and loaded with 4 μmol/L LysoSensor Yellow/Blue DND-160 of DMEM for 15–30 min at 37 ℃. Then, the cells were washed 3 times with PBS buffer and immediately observed by fluorescence microscopy (Japan). At least 3 biologically independent experiments were conducted.

2.7. Detection of lysosomal degradation capacity

The DQ™-Green-BSA Kit (Thermo Fisher) was used according to the manufacturer's protocol. Briefly, cells were seeded on coverslips in a 24-well plate and treated with NaF for 24 h, then incubated with DQ™-Green-BSA working solution (15 μg/ml) for 4 h, and given the designated treatment. After washing with PBS buffer 3 times, the cells were immediately observed by fluorescence microscopy (Japan). Fluorescence intensity of DQ™-Green-BSA was quantified with Image J software (Image J. NIH), lysosomal degradation expressed as the relative value of fluorescence intensity. At least 3 biologically independent experiments were conducted.

2.8. Cathepsins D (Cath-D) activity assay

The Cath-D activity was measured using commercially available kits (Yeasen). The homogenized hippocampal tissue and the treated cells were centrifuged for 15 min at 4 ℃, then the supernatant was collected, respectively. Then, 10 μL of preprocessed sample and 40 μL of sample dilution were added to the wells in an enzyme-linked immunosorbent assay plate, and 100 μL of enzyme reagent was added to each well. The plate was sealed with a porous sealing film and incubated at 37 ℃ for 60 min. The plate was washed 5 times with washing buffer. Incubated with 50 μL chromogenic agent A, mixed and avoided light for 15 min at 37 ℃. Finally, 50 μL of stopping solution was added to stop the reaction (blue turns yellow at this time). Measured optical density of samples at 450 nm (OD 450 nm) using a microplate reader (USA). Sample Cath-D activity was calculated from a standard curve. At least 3 biologically independent experiments were conducted.

2.9. Western blot analysis

Cells or hippocampus were lysed in RIPA buffer supplemented with 1% protease inhibitor. Total protein was measured, SDS–PAGE (sodium dodecyl sulfate-polyacrylamide gel electrophoresis) was used to separate the proteins, and the proteins were transferred to polyvinylidene fluoride (PVDF) membranes. Then, the PVDF membranes were incubated with 5% skim milk for 2 h at room temperature, and incubated with primary antibodies for 14–16 h at 4 ℃ (LC3 (1:500), p62 (1:1000), PARP (1:1000), V-ATPase B2 (1:1000), Cath-D (1:1000)). The membranes were washed 3 times and at room temperature incubated with secondary antibodies (1:40000) for 2 h. After washing 3 times, the membranes were observed by enhanced chemiluminescence (ECL) solution, which the intensity of the bands was quantified with Image J software (Image J. NIH). The density of each band was normalized to its respective control (β-actin or GAPDH). At least 3 biologically independent experiments were conducted.

2.10. Detection of autophagic flux

The mRFP-GFP-LC3 adenoviral vectors was used to monitor autophagic flux. SH-SY5Y cells infected with mRFP-GFP-LC3 adenovirus (MOI = 400) for 12 h at 37 ℃, then cultured with NaF (20, 40, or 60 mg/L) for another 24 h. The mRFP-GFP-LC3 distribution in SH-SY5Y cells were analyzed by fluorescence microscope (Japan) and quantified using Image J software. At least 3 biologically independent experiments were conducted.

2.11. Flux cytometry

Cells in culture dishes were washed 2 times with pre-chilled PBS buffer, cultured cells were digested with EDTA-free trypsin and collected by centrifugation. Cells were washed 2 times with pre-chilled PBS buffer and incubated with binding buffer. Then, 5 μL annexin V-FITC (Fluoresceine isothiocyanate) was added, mixed well, covered with aluminum foil to protect it from light, and reacted for 5 min. Then, 10 μL PI (propidium iodide) was added, kept away from light, and reacted for 5 min. Then, the cells were examined by a flux cytometry system (USA). At least 3 biologically independent experiments were conducted.

2.12. Statistical analysis

The data are presented as the mean ± standard deviation (SD) from independent experiments and were analyzed using SPSS 20.0. The data of the MWM test were analyzed by repeated-measures analysis of variance, and the other data were compared using one-way analysis of variance (ANOVA) followed by the Tukey test. Statistical significance was defined as $P < 0.05$.

3. Results

3.1. NaF impaired learning and memory in rat offspring

MWM was used to assess the effects of NaF on the learning and memory ability of rats. With respect to PNT of MWM, the swimming speed of the 100 mg/L NaF-treated group on the first day was significantly lower than that of the control group ($P < 0.05$; Fig. S1A), the average escape latency and swimming distance of offspring rats exposed to 100 mg/L NaF were significantly longer than those of the control group each day ($P < 0.05$; Fig. S1B-C). For the SPT of the MWM, the frequency of platform crossings, the target time ratio, and the target distance ratio of 50 and 100 mg/L NaF-treated offspring rats were significantly lower than those of the control group, respectively ($P < 0.05$; Fig. S1E-G). Fig. S1D and S1H show typical routes in the PNT and SPT, respectively. These results suggest that NaF induces impairment in learning as well as spatial exploration ability in rat offspring.

3.2. NaF induces excessive apoptosis in vitro and in vivo

To estimate the damaging effects of NaF on neuronal cells, we used Nissl staining and Western blot to detect the related apoptosis indexes. Our results showed that the protein expression levels of cleaved PARP in NaF-treated groups were dramatically increased compared with those in the control group ($P < 0.05$; Fig. 1A-B). Additionally, Nissl bodies vacuolized and decreased in the 25, 50, and 100 mg/L NaF-treated groups compared with the control group (Fig. 1C). In vitro, NaF dramatically increased the protein levels of cleaved PARP compared with the control group ($P < 0.05$; Fig. 1D-E). These results suggest that NaF causes excessive apoptosis of neuronal cells as well as damage to Nissl bodies.

3.3. Exposure to NaF induces autophagic flux blockage in vitro and in vivo

We explored the role of NaF on autophagic flux by measuring the indicators of autophagy, protein 1 A/1B-light chain 3 (LC3-II) and sequestosome 1 (p62) using western blot. Our results showed that NaF dose-dependently increased the protein levels of LC3-II and p62 in rat hippocampus and SH-SY5Y cells, compared with the control group ($P < 0.05$; Fig. 2A-D). To further validate the effects on autophagic flux induced by NaF, SH-SY5Y cells were infected with mRFP-GFP-LC3 adenovirus, which allows for discriminate autophagosomes (yellow puncta in merged image) and autolysosomes (red puncta in merged image). Our data showed that NaF increased the number of yellow puncta and decreased the number of red puncta, compared with the control group ($P < 0.05$), yet the number of green puncta also gradually increased ($P < 0.05$; Fig. 2E-F). Altogether, these results suggest that NaF causes an increase in autophagosomes as well as abnormal degradation of autophagic substrates leading to autophagic flux blockage.

3.4. NaF impairs lysosomal degradation capacity in vitro and inhibits Cath-D activity in vitro and in vivo

We used Cath-D activity kits and DQ-Green-BSA to respectively verify whether NaF inhibits Cath-D activity and lysosomal degradation capacity. The activities of Cath-D in the hippocampus were significantly decreased as the NaF concentration increased compared with the controls ($P < 0.05$; Fig. 3A). Sodium fluoride significantly and dose-dependently decreased Cath-D activity in SH-SY5Y, compared with control cells *in vitro* ($P < 0.05$; Fig. 3B). Moreover, lysosomal degradation capacity was inhibited in cells treated with NaF ($P < 0.05$; Fig. 3C-D).

3.5. NaF increases lysosomal pH in vitro

LysoSensor™ Yellow/Blue DND-160 was used to monitor alterations in lysosomal pH caused by NaF in SH-SY5Y cells. The pH increased along with enhanced blue fluorescence, particularly in 40 and 60 mg/L NaF-treated group (Fig. 4A). These results suggest that NaF exposure elevated lysosomal pH in SH-SY5Y cells.

3.6. NaF inhibited V-ATPase B2 expression in vitro and in vivo

To verify the impairment of V-ATPase by NaF, we used Western blot to test related indicators. *In vivo*, our results revealed that the expression of V-ATPase B2 was decreased in the 25, 50, and 100 mg/L NaF-treated groups, compared with the control group ($P < 0.05$; Fig. 4B-C). *In vitro*, compared with the control group, NaF inhibited the expression of V-ATPase B2 ($P < 0.05$; Fig. 4D-E), These results suggest that NaF exposure impairs the function of V-ATPase.

3.7. V-ATPase B2 overexpression restored lysosomal pH and degradation capacity inhibited by NaF in vitro

To verify whether the NaF-induced increase in lysosomal pH could be alleviated by Ad-V-ATPase B2, we tested the relevant indicators after intervention. As shown in Fig. S2A-C, Ad-V-ATPase B2 and ATP both significantly increased the protein levels of V-ATPase B2 and Cath-D in the cotreatment group (Ad-V-ATPase B2 + 60 mg/L NaF group, or ATP + 60 mg/L NaF group) compared with the 60 mg/L NaF-treated group ($P < 0.05$). Subsequently, we utilized BaF, a specific inhibitor of V-ATPase, to alkalize lysosomes. Both BaF and NaF inhibited the activity of Cath-D, and the combined effect of NaF and BaF cotreatment group was more pronounced than NaF alone ($P < 0.05$). Additionally, the activity of Cath-D inhibited by NaF was restored by Ad-V-ATPase B2 and ATP in the cotreatment group compared with the 60 mg/L NaF-treated group ($P < 0.05$; Fig. 5A). The lysosomal pH of NaF-treated cells was reversed by Ad-V-ATPase B2 compared with the 60 mg/L NaF-treated group (Fig. 5C). Furthermore, NaF-induced lysosomal degradation capacity damage (decreased green fluorescence) was recovered by Ad-V-ATPase B2 (Fig. 5B and 5D). These results suggest that V-ATPase B2 overexpression restores lysosomal pH and lysosomal degradation inhibited by NaF.

3.8. V-ATPase B2 overexpression alleviated autophagic flux blockage and apoptosis induced by NaF in vitro

To verify that Ad-V-ATPase can alleviate NaF-induced excessive apoptosis and autophagic flux blockage by restoring lysosomal pH and degradation capacity, we analyzed autophagy-related proteins (LC3-II and p62) and apoptosis rate after the intervention. As shown in Fig. 6A-C, we assessed the protein levels of p62 and LC3-II. NaF-induced increased protein levels were significantly reduced by Ad-V-ATPase B2 and ATP compared with the 60 mg/L NaF-treated group, respectively ($P < 0.05$). BaF increased the protein levels of p62 and LC3-II compared with the control group ($P < 0.05$). The BaF and NaF cotreatment group had increased protein levels of p62 and LC3-II compared with the 60 mg/L NaF-treated group ($P < 0.05$). Subsequently, our results

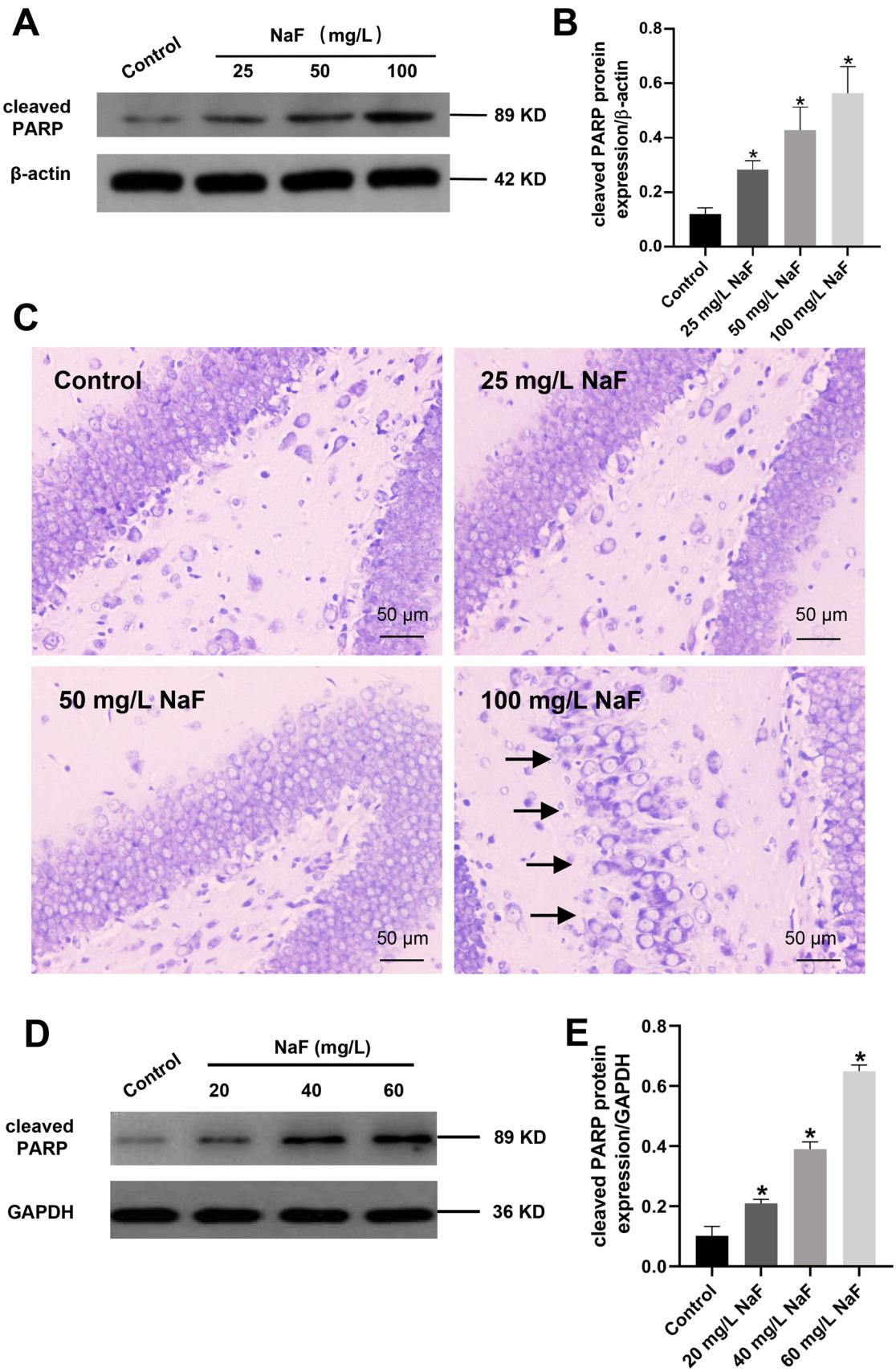

Fig. 1. NaF exposure induces excessive apoptosis *in vitro* and *in vivo*. (A) The protein expression level of Cleaved PARP in rat hippocampus. (B) Quantitative analysis for protein expression of Cleaved PARP in rat hippocampus. (C) The Nissl staining in rat hippocampus. The black arrow points to cavitation. (D) The protein expression level of Cleaved PARP in SH-SY5Y cells. (E) Quantitative analysis for protein expression of Cleaved PARP in SH-SY5Y cells. All experiments were performed independently and repeated three times. The data were presented as the means ± SD. * $P < 0.05$ compared with the control group.

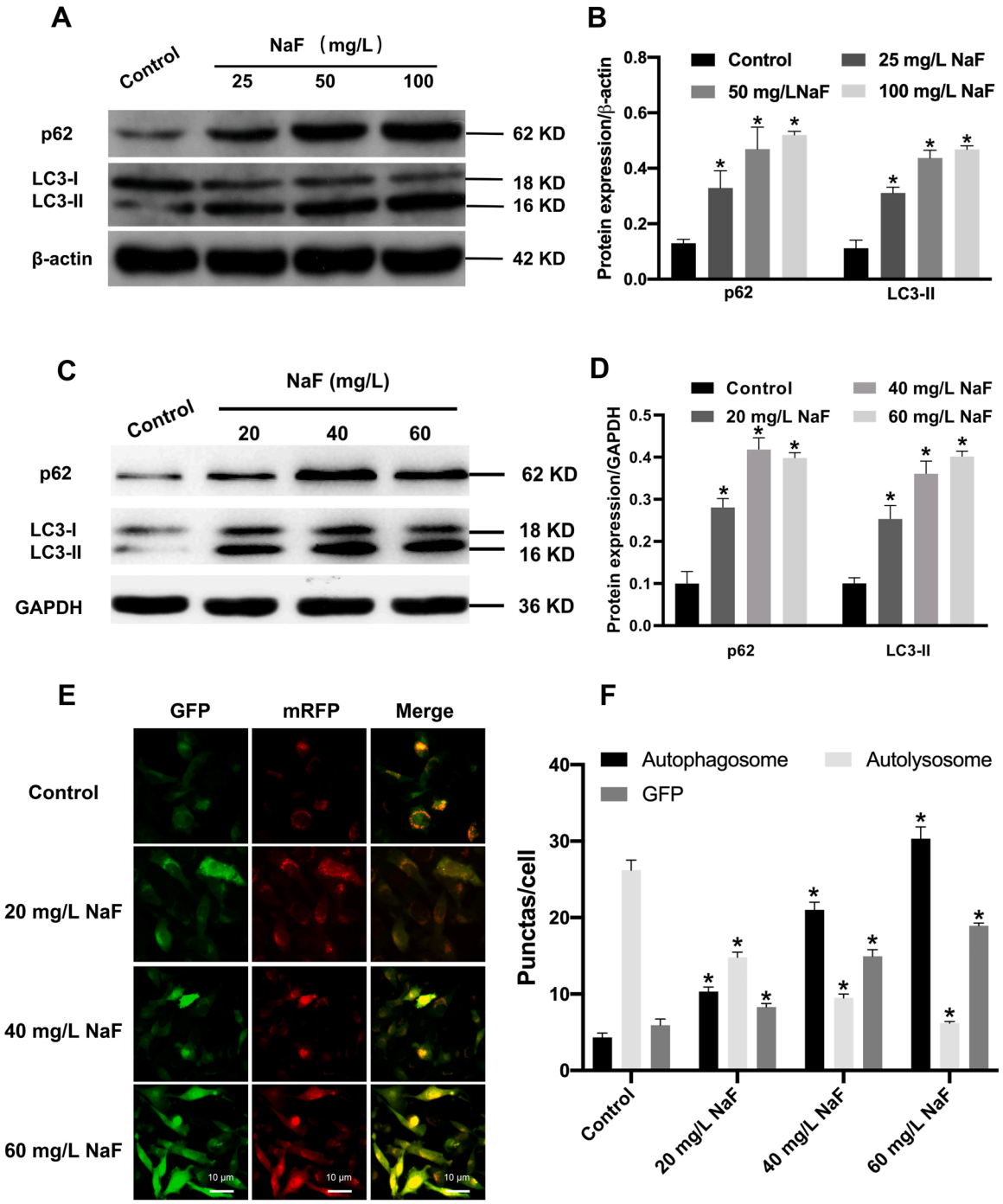

Fig. 2. NaF exposure induces autophagic flux blockage *in vitro* and *in vivo*. (A) The protein expression level of p62, and LC3-II in rat hippocampus. (B) Quantitative analysis of p62, and LC3-II in rat hippocampus. (C) The protein expression level of p62 and LC3-II in SH-SY5Y cells. (D) Quantitative analysis of p62 and LC3-II in SH-SY5Y cells. (E) SH-SY5Y cells were transfected by a mRFP-GFP-LC3 adenovirus and followed by NaF treatment (F) Quantification of autophagosomes, autolysosomes and GFP in E. All experiments were performed independently and repeated three times. The data were presented as the means ± SD. * $P < 0.05$ compared with the control group.

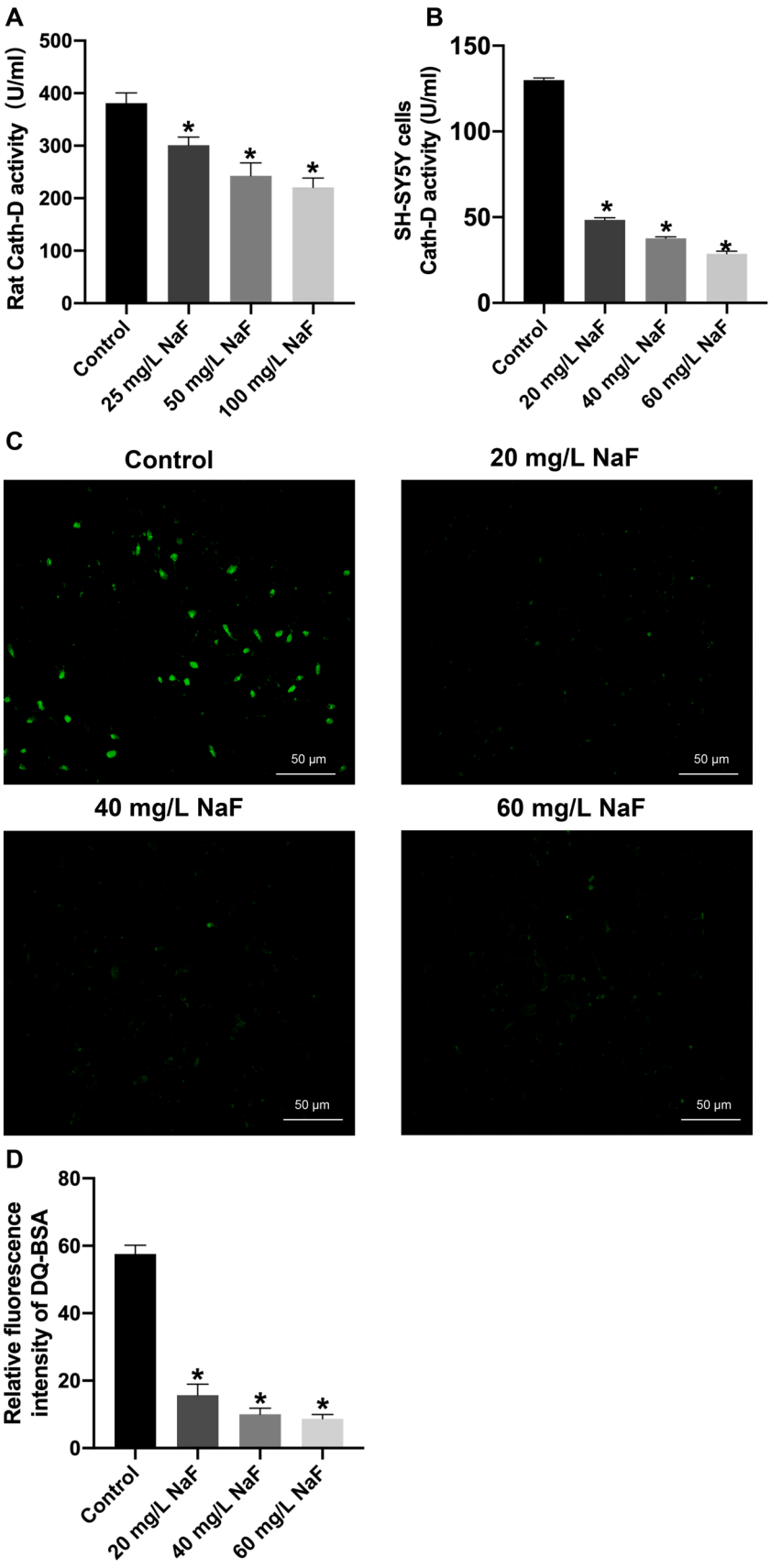

Fig. 3. NaF exposure impairs lysosomal degradation capacity *in vitro* and inhibits the activity of Cath-D *in vitro* and *in vivo*. (A) The activity of Cath-D in rat hippocampus. (B) The activity of Cath-D in SH-SY5Y cells. (C) DQ-Green BSA assay of lysosomal degradation capacity in SH-SY5Y cells. (D) The fluorescence intensity of DQ™-Green-BSA was quantified with Image J software. All experiments were performed independently and repeated three times. The data were presented as the means ± SD. * $P < 0.05$ compared with the control group.

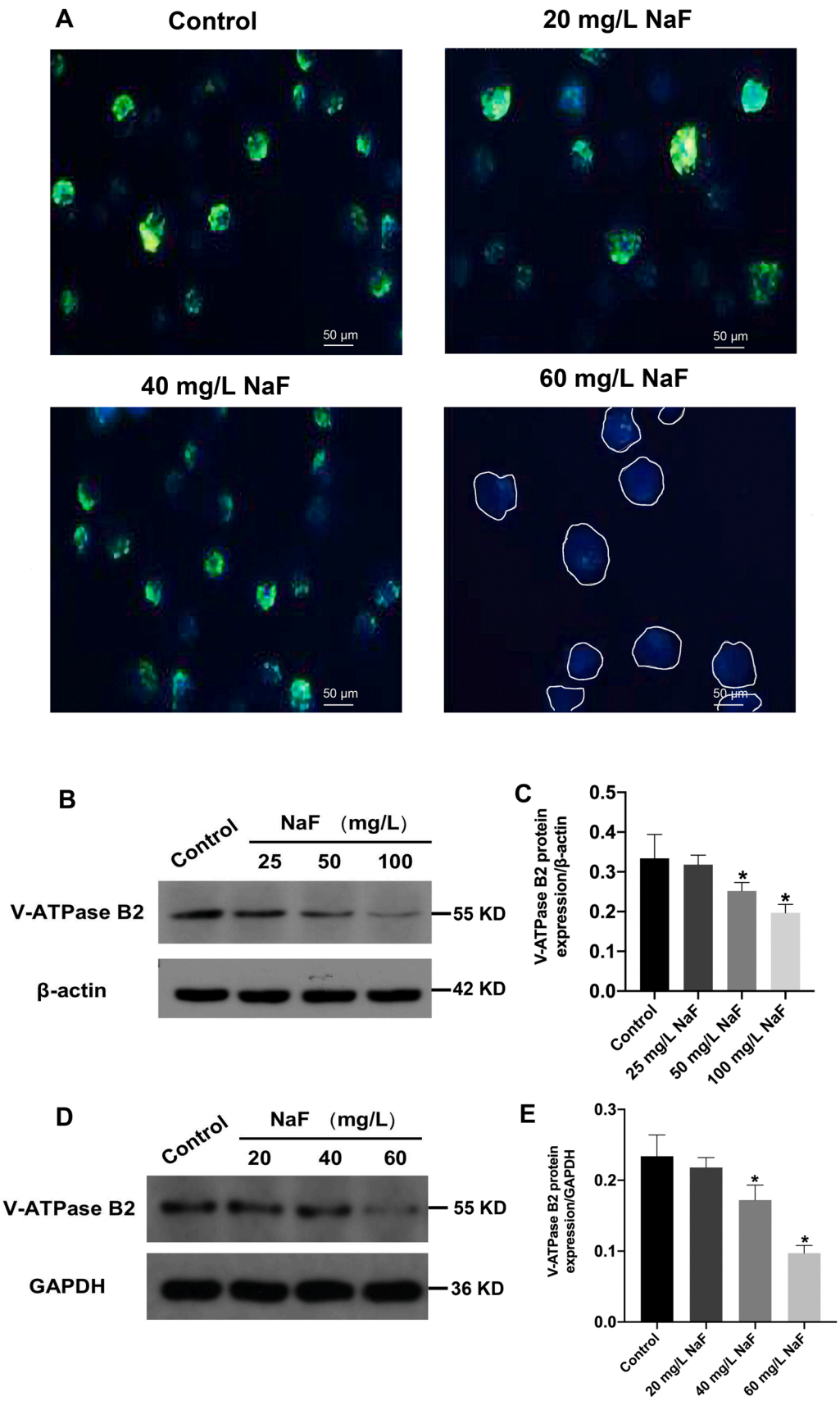

Fig. 4. NaF exposure raises lysosomal pH *in vitro* and inhibits the expression of V-ATPase B2 and the activity of V-ATPase *in vitro* and *in vivo*. (A) Lysosomal pH measurement in SH-SY5Y cells. (B) The protein expression level V-ATPase B2 in rat hippocampus. (C) Quantitative analysis of V-ATPase B2 in rat hippocampus. (D) The protein expression level of V-ATPase B2 in SH-SY5Y cells. (E) Quantitative analysis of V-ATPase B2 in SH-SY5Y cells. All experiments were performed independently and repeated three times. The data were presented as the means ± SD. * $P < 0.05$ compared with the control group.

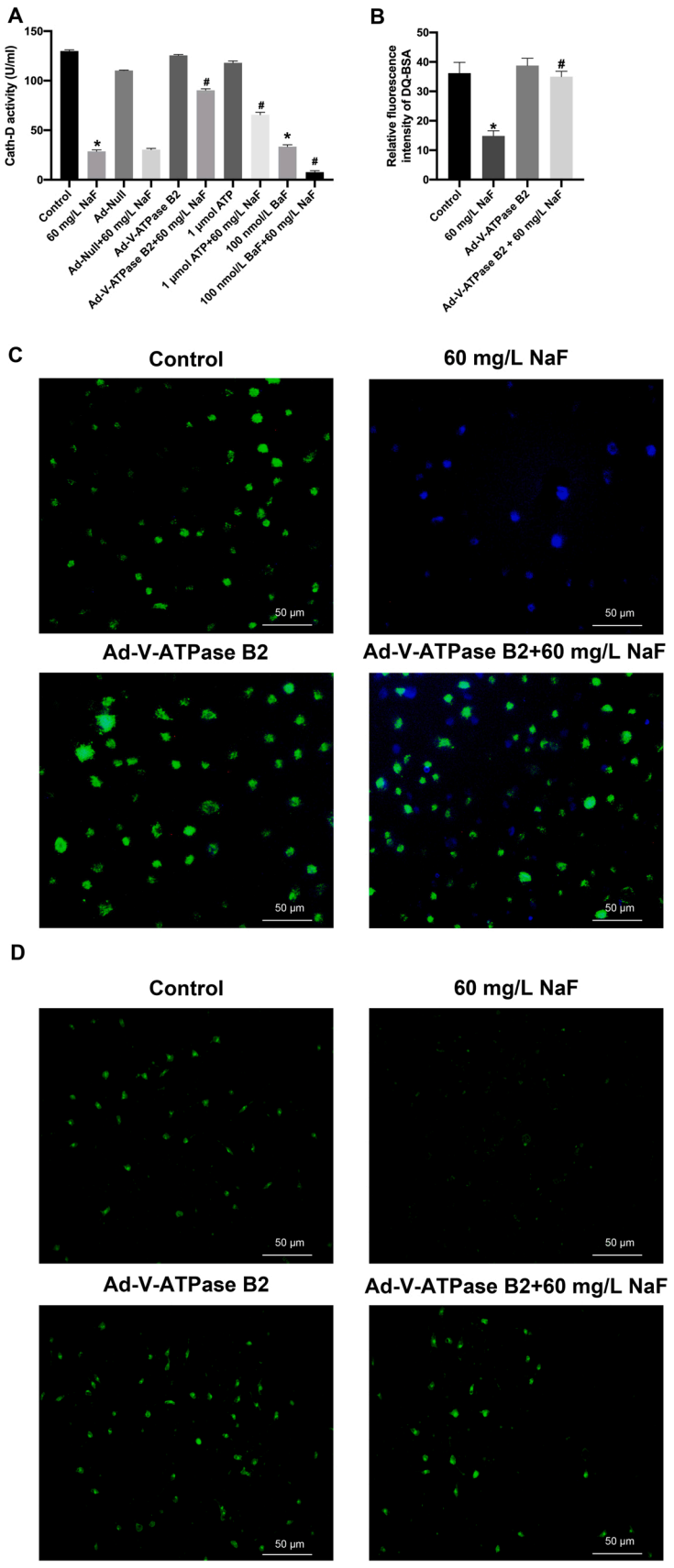

Fig. 5. V-ATPase B2 overexpression restore lysosomal pH and lysosomal degradation capacity inhibited by NaF *in vitro*. (A) The activity of Cath-D in SH-SY5Y cells. (B) The fluorescence intensity of DQ™-Green-BSA was quantified with Image J software. (C) The lysosomal pH after Ad-V-ATPase B2 treatment in SH-SY5Y cells. (D) The lysosomal degradation capacity after Ad-V-ATPase B2 treatment in SH-SY5Y cells. All experiments were performed independently and repeated three times. The data were presented as the means ± SD. * $P < 0.05$ compared with the control group, $^{\#}P < 0.05$ compared with the 60 mg/L NaF group.

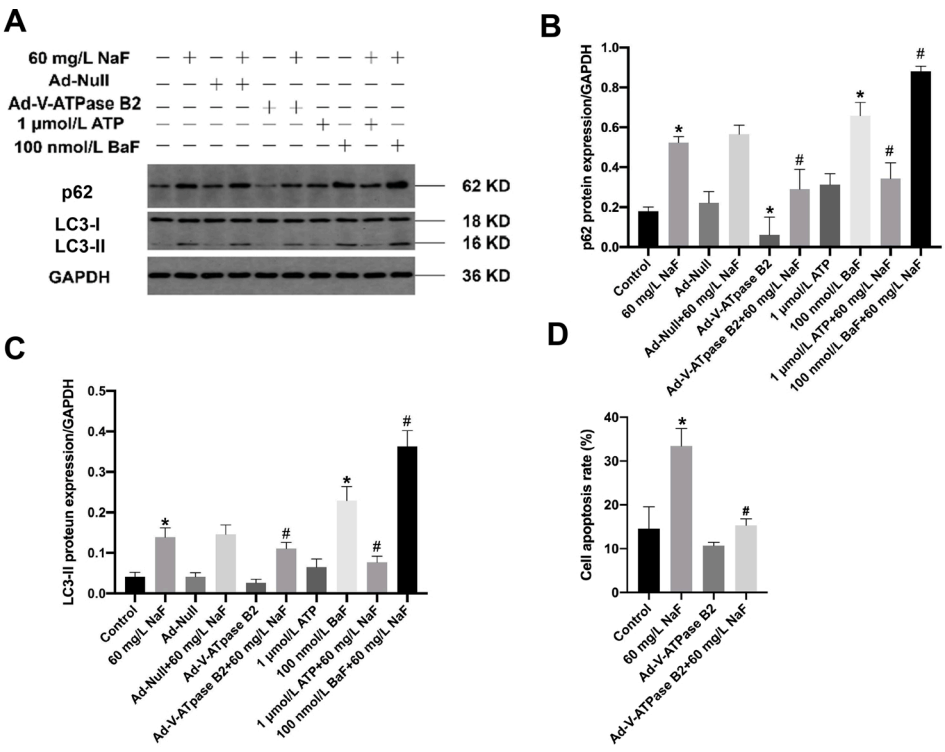

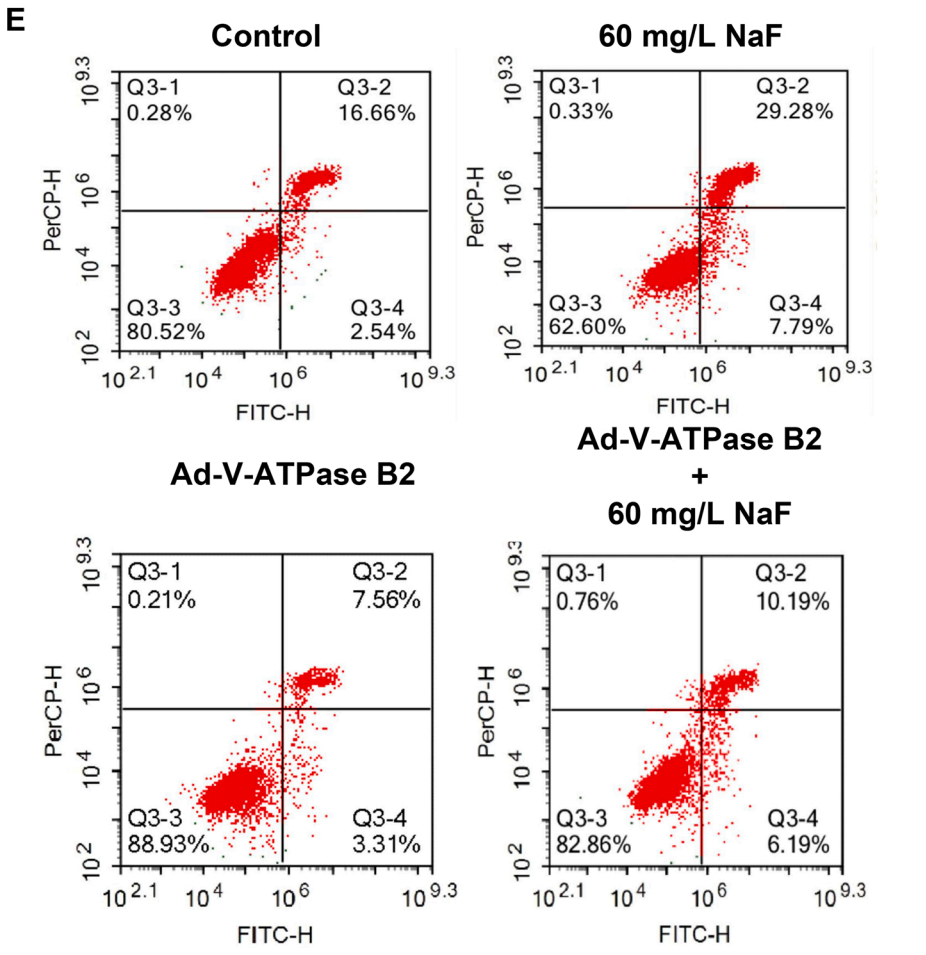

Fig. 6. V-ATPase B2 overexpression alleviated autophagic flux blockage and apoptosis induced by NaF *in vitro*. (A) The protein expression level of p62 and LC3-II in SH-SY5Y cells. (B) Quantitative analysis of p62 in SH-SY5Y cells. (C) Quantitative analysis of LC3-II in SH-SY5Y cells. (D) Quantitative analysis of results of flux cytometry in SH-SY5Y cells. (E) Flux cytometry detection of apoptosis in SH-SY5Y cells. All experiments were performed independently and repeated three times. The data were presented as the means ± SD. $^{*}P < 0.05$ compared with the control group, $^{\#}P < 0.05$ compared with the 60 mg/L NaF group.

showed that the NaF-induced apoptosis rate was significantly decreased by Ad-V-ATPase B2 in the cotreatment group compared with the 60 mg/L NaF-treated group, respectively ($P < 0.05$; Fig. 6D-E). These results suggest that V-ATPase B2 overexpression improved autophagic flux and reduced apoptosis in NaF-treated SH-SY5Y cells.

4. Discussion

Compelling evidence collectively supports that fluoride is a developmental neurotoxicant (Dórea, 2021). Thus, we developed a rat model to simulate real-world exposure to fluoride at the stages of brain development from embryo to maturity. We found that NaF exposure during the critical period of nervous system development resulted in impaired learning and memory capacities in rats. The present results are consistent with previous studies showing that exposure to NaF from gestation to adulthood at comparable dosages (100 mg/L) resulted in prolonged escape latency and increased swimming distance in rat offspring (Qiu et al., 2020). Interestingly, these findings are consistent with epidemiological studies showing that fluorosis patients born and raised in fluorosis areas have poorer memory and cognitive abilities (Wang et al., 2007). Thus, the present results reconfirm and provide evidence that NaF is a developmental neurotoxicant.

The mechanism of fluoride-induced developmental neurotoxicity remains unknown, and apoptosis is considered to be a significant cause of neuron loss. In the present study, we found that NaF causes neuronal damage in the hippocampal CA3 region of rat offspring, as evidenced by disorderly arrangement, and reduction in the number of Nissl bodies. The Nissl body mainly synthesizes proteins to replenish the protein consumption of neurons during excitation transmission. Under physiological conditions, neurons are more capable of synthesizing proteins, and therefore large and numerous Nissl bodies are visible by Nissl staining, whereas neurons are damaged, the number of Nissl bodies decreases or even disappears (Tian and Brainard, 2017). Based on the above findings, we are confident that NaF causes the development of neurotoxicity by destroying Nissl bodies, resulting in neuronal loss. The present findings also provide persuasive evidence to support NaF-induced neuronal apoptosis, which was proven by the increased PARP cleavage *in vivo* and *in vitro*. These findings are in line with a recent study on hippocampal neuron loss and apoptosis in a fluoride-exposed rat model (Jiang et al., 2019). Briefly, the present results suggest that NaF-induced excessive apoptosis participates in fluoride neurodevelopmental toxicity.

Autophagy is crucial for the development of the nervous system as well as in sustaining neuronal homeostasis (Kulkarni et al., 2018). Here, we found increased LC3-II levels *in vivo* and *in vitro*, as LC3-II levels directly correlate with the number of mature autophagosomes (Kabeya et al., 2000), the results suggest that NaF triggers the accumulation of autophagosomes. The specific autophagic degradation substrate, p62, was also dose-dependently elevated in response to NaF *in vivo* and *in vitro*. The LC3-interacting region (LIR) of p62 interacts with multiple sites on LC3 to deliver ubiquitinated substrates into complete autophagosomes, where they are degraded in autophagic lysosomes (Jatana et al., 2020). Elevated LC3-II expression and accumulated p62 are attributed to impaired autophagosomal degradation (Komatsu and Ichimura, 2010; Xiong et al., 2014). Consistently, the number of yellow and green puncta gradually increased in NaF-treated mRFP-GFP-LC3 transfected SH-SY5Y cells *in vitro*, while the number of red puncta denote the opposite trend. These results indicate that NaF caused an increase in autophagosomes and inhibit the fusion of autophagosomes with lysosomes, also led to an increase in the pH of lysosomes thus causing autophagic flux blockage. Therefore, the present results suggest that impaired autophagic degradation is likely to be an important cause of NaF-induced developmental neurotoxicity.

Lysosomes is the terminal end of autophagic flux, through which substances within the autophagosomes are degraded and recycled, thus contributing to cellular homeostasis (Banerjee and Kane, 2020). Lysosomal degradation capacity is primarily determined by hydrolase activity. Interestingly, our findings revealed that NaF exposure decreased Cath-D activity *in vivo* and *in vitro*. Correspondingly, we found that NaF exposure reduced lysosomal degradation capacity, as indicated by DQ™-Green-BSA fluorescence intensity. Cath-D is a lysosomal aspartate protease that is activated at low pH and digests substances in the lysosome to sustain cellular homeostasis (Tran and Silver, 2021; Marques et al., 2020). The loss of Cath-D leads to lysosomal dysfunction and the accumulation of different cellular proteins associated with neurodegenerative diseases (Hossain et al., 2021). Overall, our findings indicated that NaF could reduce Cath-D activity and expression and thus diminish the lysosomal degradation capacity in neurons. In addition, lysosomes have a critical requirement for low pH, and the acidic environment within the lysosomal lumen promotes the degradation of misfolded proteins and damaged organelles and provides the optimal microenvironment for various hydrolases (Hadi et al., 2021). Surprisingly, the present study results showed that NaF exposure elevated the lysosomal pH of SH-SY5Y cells, with a dose-effect relationship. Kazushi Aoto (Aoto et al. (2021) discovered that increased lysosomal pH affects human and mouse brain development. A similar finding was obtained from a recent study that raised lysosomal pH produced defects in hydrolase capacity (Ponsford et al., 2021). Considering the findings mentioned above, it is conceivable that NaF exposure altered the hydrolase-dependent environment by elevating the pH of the lysosomal lumen, resulting in a diminution in lysosomal degradation capacity.

The proton pump V-ATPase maintains a low pH in the lysosomal membrane (Li et al., 2021). V-ATPase is a multisubunit complex that hydrolyzes ATP and transports hydrogen ions to lysosomes, which stabilizes the lysosomal pH (Lee et al., 2015). The role of V-ATPase in the increased lysosomal pH induced by fluoride remains unclear. Here, NaF exposure resulted in reduced V-ATPase expression in SH-SY5Y cells, suggesting that NaF may cause lysosomal luminal pH increase by inhibiting the expression of V-ATPase. To further investigate the role of V-ATPase in NaF-induced developmental neurotoxicity, we used ATP (a substrate of V-ATPase) and BaF (a specific inhibitor of V-ATPase) to explore the role of V-ATPase in NaF-treated SH-SY5Y cells. Supportively, ATP treatment enhanced, while BaF inhibited, the protein level of the V-ATPase B2. Furthermore, Ad-V-ATPase B2 increased V-ATPase B2 expression, and alleviated lysosomal alkalinization in SH-SY5Y cells incubated with NaF. Since the acidic microenvironment in lysosomes is an essential prerequisite for hydrolases to perform their degradation functions, we further analyzed the expression and activity of lysosomal hydrolases after V-ATPase B2 overexpression. As predicted, Ad-V-ATPase B2 effectively alleviated the NaF-induced suppression of Cath-D activity and expression levels and prevented the suppression of NaF-induced lysosomal degradation capacity. Taken together, our experimental results revealed that the NaF-induced reduction in lysosomal V-ATPase expression was mitigated by Ad-V-ATPase B2, which ensured the normal lysosomal acidification process, thereby creating an appropriate microenvironment for hydrolase degradation and promoting lysosomal degradation capacity. Autophagic flux is determined by the restoration of lysosomal degradation capacity function (Kaminskyy and Zhivotovsky, 2012). We also provide the results that after Ad-V-ATPase B2 treatment, the high expression of both autophagic degradation substrate p62 and autophagic vesicle marker protein LC3-II declined due to enhanced lysosomal degradation capacity. Sergin et al. (2017) discovered that restoring lysosomal degradation capacity in atherosclerosis may efficiently reduce p62 aggregation and block macrophage apoptosis, which is related to reduced atherosclerosis. The present findings thus suggest that NaF-induced impairment of autophagic degradation may be reversed by restoring lysosomal degradation capacity function through Ad-V-ATPase B2, which restored autophagic flux. Encouragingly, we also found that Ad-V-ATPase B2 alleviated excessive neuronal apoptosis. Lead-induced cytotoxicity in rat renal tubular epithelial cells restores autophagic flux by increasing lysosomal degradation capacity, which consequently decreases apoptosis (Song

et al., 2017). Our results suggested that targeting V-ATPase and sustaining robust autophagic flux might be key to minimizing fluoride-induced apoptosis.

In conclusion, we provided the first evidence that NaF induces developmental neurotoxicity by decreasing lysosomal V-ATPase expression, increasing lysosomal pH, disrupting lysosomal degradation capacity, and blocking autophagic flux, induced neurotoxicity. In particular, the above changes caused by NaF can be effectively alleviated by targeting V-ATPase to restore the acidic environment of the lysosomal lumen, promote Cath-D activity and expression, and enhance lysosomal degradation capacity, thereby sustaining robust autophagic flux and reducing excessive apoptosis of neurons. In this context, V-ATPase might serve as a critical target of fluoride-induced developmental neurotoxicity. This could be a novel strategy to prevent and control fluoride-induced developmental neurotoxicity.

CRediT authorship contribution statement

Xie Han: Methodology, Formal analysis, Writing – original draft. **Yanling Tang:** Methodology, Writing – review & editing. **Yuanli Zhang:** Writing – review & editing. **Jingjing Zhang:** Visualization, Investigation. **Zeyu Hu:** Visualization, Investigation. **Wanjing Xu:** Investigation. **Shangzhi Xu:** Writing – review & editing. **Qiang Niu:** Conceptualization, Resources, Writing – review & editing, Funding acquisition.

Declaration of Competing Interest

The authors declare that they have no known competing financial interests or personal relationships that could have appeared to influence the work reported in this paper.

Acknowledgments

This work was supported by grants from the National Natural Science Foundation of China (Grant No. 81860559 and Grant No. 82060580), the Program of Science and Technology Innovation in Bingtuan (Grant No. 2021CB046), and the High-Level Talent Research Project of Shihezi University (Grant No. RCZK2018C02).

Appendix A. Supporting information

Supplementary data associated with this article can be found in the online version at doi:10.1016/j.ecoenv.2022.113500.

References

Aoto, K., Kato, M., Akita, T., Nakashima, M., Mutoh, H., Akasaka, N., Tohyama, J., Nomura, Y., Hoshino, K., Ago, Y., Tanaka, R., Epstein, O., Ben-Haim, R., Heyman, E., Miyazaki, T., Belal, H., Takabayashi, S., Ohba, C., Takata, A., Mizuguchi, T., Miyatake, S., Miyake, N., Fukuda, A., Matsumoto, N., Saitsu, H., 2021. ATP6V0A1 encoding the a1-subunit of the V0 domain of vacuolar H(+)-ATPases is essential for brain development in humans and mice. Nat. Commun. 12 (1), 2107. https://doi.org/10.1038/s41467-021-22389-5.

Atlanta. Agency for Toxic Substances and Disease Registry (ATSDR), 2003. Toxicol. Profile Fluorides, Hydrog. Fluoride Fluor. (Update). ⟨https://www.atsdr.cdc.gov/es/toxfaqs /es_tfacts11.html⟩.

Avvannavar, S.M., 2007. Sci. Total Environ. 382 (2), 388. https://doi.org/10.1016/j.scitotenv.2007.03.038.

Banerjee, S., Kane, P.M., 2020. Regulation of V-ATPase activity and organelle ph by phosphatidylinositol phosphate Lipids. Front Cell Dev. Biol. 8, 510. https://doi.org/10.3389/fcell.2020.00510.

Blumenreich, S., Barav, O.B., Jenkins, B.J., Futerman, A.H., 2020. Lysosomal storage disorders shed light on lysosomal dysfunction in Parkinson's disease. Int J. Mol. Sci. 21 (14) https://doi.org/10.3390/ijms21144966.

Cao, K., Xiang, J., Dong, Y.T., Xu, Y., Li, Y., Song, H., Zeng, X.X., Ran, L.Y., Hong, W., Guan, Z.Z., 2019. Exposure to fluoride aggravates the impairment in learning and memory and neuropathological lesions in mice carrying the APP/PS1 double-transgenic mutation. Alzheimers Res Ther. 11 (1), 35. https://doi.org/10.1186/s13195-019-0490-3.

Colacurcio, D.J., Nixon, R.A., 2016. Disorders of lysosomal acidification-The emerging role of v-ATPase in aging and neurodegenerative disease. Ageing Res Rev. 32, 75–88. https://doi.org/10.1016/j.arr.2016.05.004.

Dec, K., łukomska, A., Maciejewska, D., Jakubczyk, K., Baranowska-Bosiacka, I., Chlubek, D., Wąsik, A., Gutowska, I., 2017. The influence of fluorine on the disturbances of homeostasis in the central nervous system. Biol. Trace Elem. Res 177 (2), 224–234 https://doi.org/10. 1007/s12011-1016.

Dobbing, J., 1971. Vulnerable periods of brain development. In: lipids, malnutrition & the developing brain. Ciba Found. Symp. 9–29.

Dórea, J.G., 2021. Exposure to environmental neurotoxic substances and neurodevelopment in children from Latin America and the Caribbean. Environ. Res. 192, 110199 https://doi.org/10.1016/j.envres.2020.110199.

Gao, Q., Liu, Y.J., Guan, Z.Z., 2008. Oxidative stress might be a mechanism connected with the decreased alpha 7 nicotinic receptor influenced by high-concentration of fluoride in SH-SY5Y neuroblastoma cells. Toxicol. Vitr. 22 (4), 837–843. https://doi.org/10.1016/j.tiv.2007.12.017.

Goschorska, M., Baranowska-Bosiacka, I., Gutowska, I., Tarnowski, M., Piotrowska, K., Metryka, E., Safranow, K., Chlubek, D., 2018. Effect of acetylcholinesterase inhibitors donepezil and rivastigmine on the activity and expression of cyclooxygenases in a model of the inflammatory action of fluoride on macrophages obtained from THP-1 monocytes. Toxicology 406–407, 9–20. https://doi.org/10.1016/j.tox.2018.05.007.

Hadi, M.M., Nesbitt, H., Masood, H., Sciscione, F., Patel, S., Ramesh, B.S., Emberton, M., Callan, J.F., Macrobert, A., Mchale, A.P., Nomikou, N., 2021. Investigating the performance of a novel pH and cathepsin B sensitive, stimulus-responsive nanoparticle for optimised sonodynamic therapy in prostate cancer. J. Control Release 329, 76–86. https://doi.org/10.1016/j.jconrel.2020.11.040.

Hossain, M.I., Marcus, J.M., Lee, J.H., Garcia, P.L., Singh, V., Shacka, J.J., Zhang, J., Gropen, T.I., Falany, C.N., Andrabi, S.A., 2021. Restoration of CTSD (cathepsin D) and lysosomal function in stroke is neuroprotective. Autophagy 17 (6), 1330–1348. ⟨https://doi.org/10.1080/15548627⟩. 2020.1761219.

Jatana, N., Ascher, D.B., Pires, D., Gokhale, R.S., Thukral, L., 2020. Human LC3 and GABARAP subfamily members achieve functional specificity via specific structural modulations. Autophagy 16 (2), 239–255. https://doi.org/10.1080/15548627.2019.1606636.

Jiang, P., Li, G., Zhou, X., Wang, C., Qiao, Y., Liao, D., Shi, D., 2019. Chronic fluoride exposure induces neuronal apoptosis and impairs neurogenesis and synaptic plasticity: Role of GSK-3β/β-catenin pathway. Chemosphere 214, 430–435. https://doi.org/10.1016/j. chemosphere.2018.09. 095.

Jimenez-Moreno, N., Lane, J.D., 2020. Autophagy and redox homeostasis in Parkinson's: a crucial balancing act. Oxid. Med Cell Longev. 2020, 8865611 https://doi.org/10.1155/2020/8865611.

Johnston, N.R., Strobel, S.A., 2020. Principles of fluoride toxicity and the cellular response: a review. Arch. Toxicol. 94 (4), 1051–1069. https://doi.org/10.1007/s00204-020-02687-5.

Kabeya, Y., Mizushima, N., Ueno, T., Yamamoto, A., Kirisako, T., Noda, T., Kominami, E., Ohsumi, Y., Yoshimori, T., 2000. LC3, a mammalian homologue of yeast Apg8p, is localized in autophagosome membranes after processing. EMBO J. 19 (21), 5720–5728. https://doi.org/10.1093/emboj/19.21.5720.

Kaminskyy, V., Zhivotovsky, B., 2012. Proteases in autophagy. Biochim Biophys. Acta 1824 (1), 44–50. https://doi.org/10.1016/j.bbapap.2011.05.013.

Komatsu, M., Ichimura, Y., 2010. Physiological significance of selective degradation of p62 by autophagy. FEBS Lett. 584 (7), 1374–1378. https://doi.org/10.1016/j.febslet.2010.02.017.

Kulkarni, Aditi, Chen Jessica, Maday Sandra, 2018. Neuronal autophagy and intercellular regulation of homeostasis in the brain. Curr. Opin. Neurobiol. 51, 29–36. https://doi.org/10.1016/j.conb.2018.02.008.

Lacson, C., Lu, M.C., Huang, Y.H., 2020. Fluoride network and circular economy as potential model for sustainable development-a review. Chemosphere 239, 124662. https://doi.org/10.1016/j.chemosphere.2019.124662.

Li, X., Jiang, J., Yang, Z., Jin, S., Lu, X., Qian, Y., 2021. Galangin suppresses RANKL-induced osteoclastogenesis via inhibiting MAPK and NF-κB signalling pathways. J. Cell Mol. Med. 25 (11), 4988–5000. https://doi.org/10.1111/jcmm.16430.

Liu, X.J., Liang, X.Y., Guo, J., Shi, X.K., Merzendorfer, H., Zhu, K.Y., Zhang, J.Z., 2021. V-ATPase subunit a is required for survival and midgut development of Locusta migratoria. Insect Mol. Biol. https://doi.org/10.1111/imb.12738.

Marques, A., Di Spiezio, A., Thießen, N., Schmidt, L., Grötzinger, J., Lüllmann-Rauch, R., Damme, M., Storck, S.E., Pietrzik, C.U., Fogh, J., Bär, J., Mikhaylova, M., Glatzel, M., Bassal, M., Bartsch, U., Saftig, P., 2020. Enzyme replacement therapy with recombinant pro-CTSD (cathepsin D) corrects defective proteolysis and autophagy in neuronal ceroid lipofuscinosis. Autophagy 16 (5), 811–825. https://doi.org/10.1080/15548627.2019.1637200.

Mizushima, N., Levine, B., 2020. Autophagy in human diseases. New Engl. J. Med 383 (16), 1564–1576. https://doi.org/10.1056/NEJMra2022774.

Nie, T., Zhu, L., Yang, Q., 2021. The classification and basic processes of autophagy. Adv. Exp. Med Biol. 1208, 3–16. https://doi.org/10.1007/978-981-16-2830-6_1.

Niu, Q., Chen, J., Xia, T., Li, P., Zhou, G., Xu, C., Zhao, Q., Dong, L., Zhang, S., Wang, A., 2018. Excessive ER stress and the resulting autophagic flux dysfunction contribute to fluoride-induced neurotoxicity. Environ. Pollut. 233, 889–899. https://doi.org/10.1016/j.envpol.2017.09.015.

O'Mullane, D.M., Baez, R.J., Jones, S., Lennon, M.A., Petersen, P.E., Rugg-Gunn, A.J., Whelton, H., Whitford, G.M., 2016. Fluoride and Oral Health. Community Dent. Health 33 (2), 69–99.

Ponsford, A.H., Ryan, T.A., Raimondi, A., Cocucci, E., Wycislo, S.A., Fröhlich, F., Swan, L.E., Stagi, M., 2021. Live imaging of intra-lysosome pH in cell lines and

primary neuronal culture using a novel genetically encoded biosensor. Autophagy 17 (6), 1500–1518. https://doi.org/10.1080/15548627.2020.1771858.
Program, N.T., 2016. NTP Research Report on Systematic Literature Review on the Effects of Fluoride on Learning and Memory in Animal Studies: Research Report 1. Research Triangle Park (NC): National Toxicology Program.
Qiu, Y., Chen, X., Yan, X., Wang, J., Yu, G., Ma, W., Xiao, B., Quinones, S., Tian, X., Ren, X., 2020. Gut Microbiota Perturbations and Neurodevelopmental Impacts in Offspring Rats Concurrently Exposure to Inorganic Arsenic and Fluoride. Environ. Int 140, 105763. https://doi.org/10.1016/j.envint.2020.105763.
Rudnik, S., Damme, M., 2021. The lysosomal membrane-export of metabolites and beyond. FEBS J. 288 (14), 4168–4182. https://doi.org/10.1111/febs.15602.
Sergin, I., Evans, T.D., Zhang, X., Bhattacharya, S., Stokes, C.J., Song, E., Ali, S., Dehestani, B., Holloway, K.B., Micevych, P.S., Javaheri, A., Crowley, J.R., Ballabio, A., Schilling, J.D., Epelman, S., Weihl, C.C., Diwan, A., Fan, D., Zayed, M. A., Razani, B., 2017. Exploiting macrophage autophagy-lysosomal biogenesis as a therapy for atherosclerosis. Nat. Commun. 8, 15750. https://doi.org/10.1038/ncomms15750.
Shaikh, S., Ahmad, K., Ahmad, S.S., Lee, E.J., Lim, J.H., Beg, M., Verma, A.K., Choi, I., 2021. Natural products in therapeutic management of multineurodegenerative disorders by targeting autophagy. Oxid. Med Cell Longev. 2021, 6347792. https://doi.org/10.1155/2021/6347792.
Song, X.B., Liu, G., Liu, F., Yan, Z.G., Wang, Z.Y., Liu, Z.P., Wang, L., 2017. Autophagy blockade and lysosomal membrane permeabilization contribute to lead-induced nephrotoxicity in primary rat proximal tubular cells. Cell Death Dis. 8 (6), e2863 https://doi.org/10.1038/cddis.2017.262.
Su, H., Kang, W., Li, Y., Li, Z., 2021. Fluoride and nitrate contamination of groundwater in the Loess Plateau, China: sources and related human health risks[J]. Environ. Pollut. 286, 117287 https://doi.org/10.1016/j.envpol.2021.117287.
Tian, Lucas Y., Brainard, Michael S., 2017. Discrete circuits support generalized versus context-specific vocal learning in the songbird. Neuron 96 (5), 1168–1177. https://doi.org/10.1016/j.neuron.2017.10.019 e5.
Tran, A.P., Silver, J., 2021. Cathepsins in neuronal plasticity. Neural Regen. Res. 16 (1), 26–35. https://doi.org/10.4103/1673-5374.286948.
Trivedi, P.C., Bartlett, J.J., Pulinilkunnil, T., 2020. Lysosomal biology and function: modern view of cellular debris Bin. Cells 9 (5), 1131. https://doi.org/10.3390/cells9051131.
Valdez, J.L., López, G.O., Cervantes, F.M., Costilla-Salazar, R., Calderón, H.J., Alcaraz, C. Y., Rocha-Amador, D.O., 2017. In utero exposure to fluoride and cognitive development delay in infants. Neurotoxicology 59, 65–70. https://doi.org/10.1016/j.neuro.2016.12.011.
Wang, M., Li, X., He, W.Y., Li, J.X., Zhu, Y.Y., Liao, Y.L., Yang, J.Y., Yang, X.E., 2019. Distribution, health risk assessment, and anthropogenic sources of fluoride in farmland soils in phosphate industrial area, southwest China. Environ. Pollut. 249, 423–433. https://doi.org/10.1016/j.envpol.2019.03.044.
Wang, S.X., Wang, Z.H., Cheng, X.T., Li, J., Sang, Z.P., Zhang, X.D., Han, L.L., Qiao, X.Y., Wu, Z.M., Wang, Z.Q., 2007. Arsenic and fluoride exposure in drinking water: children's IQ and growth in Shanyin county, Shanxi province, China. Environ. Health Perspect. 115 (4), 643–647. https://doi.org/10.1289/ehp.9270.
Xin, J., Wang, H., Sun, N., Bughio, S., Zeng, D., Li, L., Wang, Y., Khalique, A., Zeng, Y., Pan, K., Jing, B., Ma, H., Bai, Y., Ni, X., 2021. Probiotic alleviate fluoride-induced memory impairment by reconstructing gut microbiota in mice. Ecotoxicol. Environ. Saf. 215, 112108 https://doi.org/10.1016/j.ecoenv.2021.112108.
Xiong, Y., Yepuri, G., Forbiteh, M., Yu, Y., Montani, J.P., Yang, Z., Ming, X.F., 2014. ARG2 impairs endothelial autophagy through regulation of MTOR and PRKAA/AMPK signaling in advanced atherosclerosis. Autophagy 10 (12), 2223–2238. ⟨https://doi.org/10.4161/15548627⟩. 2014.981789.
Yadav, K.K., Gupta, N., Kumar, V., Khan, S.A., Kumar, A., 2018. A review of emerging adsorbents and current demand for defluoridation of water: bright future in water sustainability. Environ. Int. 111, 80–108. https://doi.org/10.1016/j.envint.2017.11.014.
Yamamoto, T., Takabatake, Y., Minami, S., Sakai, S., Fujimura, R., Takahashi, A., Namba-Hamano, T., Matsuda, J., Kimura, T., Matsui, I., Kaimori, J.Y., Takeda, H., Takahashi, M., Izumi, Y., Bamba, T., Matsusaka, T., Niimura, F., Yanagita, M., Isaka, Y., 2021. Eicosapentaenoic acid attenuates renal lipotoxicity by restoring autophagic flux. Autophagy 17 (7), 1700–1713. https://doi.org/10.1080/15548627.2020.1782034.
Yu, X., Chen, J., Li, Y., Liu, H., Hou, C., Zeng, Q., Cui, Y., Zhao, L., Li, P., Zhou, Z., Pang, S., Tang, S., Tian, K., Zhao, Q., Dong, L., Xu, C., Zhang, X., Zhang, S., Liu, L., Wang, A., 2018. Threshold effects of moderately excessive fluoride exposure on children's health: a potential association between dental fluorosis and loss of excellent intelligence. Environ. Int. 118, 116–124. https://doi.org/10.1016/j.envint.2018.05.042.
Zhang, X., Wei, M., Fan, J., Yan, W., Zha, X., Song, H., Wan, R., Yin, Y., Wang, W., 2021. Ischemia-induced upregulation of autophagy preludes dysfunctional lysosomal storage and associated synaptic impairments in neurons. Autophagy 17 (6), 1519–1542. https://doi.org/10.1080/15548627.2020.1840796.
Zhao, Q., Tian, Z., Zhou, G., Niu, Q., Chen, J., Li, P., Dong, L., Xia, T., Zhang, S., Wang, A., 2020. SIRT1-dependent mitochondrial biogenesis supports therapeutic effects of resveratrol against neurodevelopment damage by fluoride. Theranostics 10 (11), 4822–4838. ⟨https://doi.org/10.7150/thno.42387⟩.
Zhou, G., Tang, S., Yang, L., Niu, Q., Chen, J., Xia, T., Wang, S., Wang, M., Zhao, Q., Liu, L., Li, P., Dong, L., Yang, K., Zhang, S., Wang, A., 2019. Effects of long-term fluoride exposure on cognitive ability and the underlying mechanisms: Role of autophagy and its association with apoptosis. Toxicol. Appl. Pharm. 378, 114608 https://doi.org/10.1016/j.taap.2019.114608.